

# Cell-Free Massive MIMO for URLLC: A Finite-Blocklength Analysis

Alejandro Lancho, *Member, IEEE*, Giuseppe Durisi, *Senior Member, IEEE*, and Luca Sanguinetti, *Senior Member, IEEE*

**Abstract**—We present a general framework for the characterization of the packet error probability achievable in cell-free Massive multiple-input multiple output (MIMO) architectures deployed to support ultra-reliable low-latency (URLLC) traffic. The framework is general and encompasses both centralized and distributed cell-free architectures, arbitrary fading channels and channel estimation algorithms at both network and user-equipment (UE) sides, as well as arbitrary combining and precoding schemes. The framework is used to perform numerical experiments on specific scenarios, which illustrate the superiority of cell-free architectures compared to cellular architectures in supporting URLLC traffic in uplink and downlink. Also, these numerical experiments provide the following insights into the design of cell-free architectures for URLLC: *i*) minimum mean square error (MMSE) spatial processing must be used to achieve the URLLC targets; *ii*) for a given total number of antennas per coverage area, centralized cell-free solutions involving single-antenna access points (APs) offer the best performance in the uplink, thereby highlighting the importance of reducing the average distance between APs and UEs in the URLLC regime; *iii*) this observation applies also to the downlink, provided that the APs transmit precoded pilots to allow the UEs to estimate accurately the precoded channel.

**Index Terms**—Cell-free Massive MIMO, finite-blocklength regime, ultra-reliable low-latency communications, centralized and decentralized operation, uplink and downlink.

## I. INTRODUCTION

One of the most challenging use cases in next-generation wireless communication systems (5G and beyond) is ultra-reliable low-latency communications (URLLC)—a novel use case aimed at providing connectivity to real-time mission-critical applications [2]. In some of the most challenging

Alejandro Lancho is with the Department of Electrical Engineering and Computer Science, Massachusetts Institute of Technology, Cambridge 02139, MA, USA (e-mail: lancho@mit.edu). Giuseppe Durisi is with the Department of Electrical Engineering, Chalmers University of Technology, Gothenburg 41296, Sweden (e-mail: durisi@chalmers.se). Luca Sanguinetti is with the Dipartimento di Ingegneria dell'Informazione, University of Pisa, 56122 Pisa, Italy (e-mail: luca.sanguinetti@unipi.it).

Alejandro Lancho has received funding from the European Union's Horizon 2020 research and innovation programme under the Marie Skłodowska-Curie grant agreement No. 101024432. This work was partly supported by the Swedish Research Council under grant 2021-04970 and by the Wallenberg AI, autonomous systems, and software program. L. Sanguinetti was partially supported by the Italian Ministry of Education and Research (MIUR) in the framework of the FoReLab projects (Departments of Excellence) and by the University of Pisa under the "PRA - Progetti di Ricerca di Ateneo" (Institutional Research Grants) - Project no. PRA-2022-2023-91 "INTERCONNECT". This work is also supported by the National Science Foundation under Grant No CCF-2131115.

The material in this paper was presented in part at the IEEE Int. Workshop Signal Process. Advances Wireless Commun. (SPAWC), Lucca, Italy, Sep. 2021. [1].

URLLC scenarios, such as factory automation, small information payloads, on the order of 100 bits, must be delivered within hundreds of microseconds and with a reliability no smaller than 99.999%. Under the stringent latency requirements of URLLC services and applications, exploiting time diversity is not possible. Furthermore, the use of frequency diversity is problematic, especially in the uplink (UL), where current standardization rules do not allow user equipments (UEs) to spread a coded packet over noncontiguous frequency resources. Hence, exploiting space diversity becomes crucial to fulfill the high reliability constraints required in URLLC. This can be achieved by the use of Massive multiple-input multiple-output (MIMO) [3], which is a key technology in 5G, owing to its ability to substantially increase the spectral efficiency [4]–[6] and the energy efficiency [7] of cellular networks. Massive MIMO refers to a wireless network where base stations (BSs), equipped with a very large number  $M$  of antennas, serve a multitude of UEs via linear spatial signal processing [8]. Important challenges in Massive MIMO are the large pathloss variations and the inter-cell interference, in particular for the cell-edge UEs [9]. These two phenomena may limit the overall network performance and prevent the use of Massive MIMO to support URLLC services.

An alternative network structure, known as cell-free Massive MIMO, was recently proposed to overcome these issues [10], [11]. In this type of network, all the UEs in a large coverage area are jointly served by multiple distributed access points (APs). The fronthaul connections between the APs and a central processing unit (CPU) enable the division of the processing tasks needed to coherently serve all the active UEs.

The majority of existing literature on cell-free Massive MIMO has been so far focused on the *ergodic regime*, where the propagation channel evolves according to a block-fading model, and one focuses on the asymptotic limit in which, as the codeword length goes to infinity, the codeword spans an arbitrarily large number of fading blocks. Unfortunately, these assumptions are highly questionable in URLLC scenarios [12]. Hence, it is unclear whether the design guidelines obtained so far for cell-free Massive MIMO [13], [14] apply to URLLC traffic.

A similar issue, but for the case of Massive MIMO cellular networks, was recently addressed in [15], where the authors presented a general framework, built on rigorous finite-blocklength information-theoretic bounds and approximations [16]–[18], to characterize the performance attainable in URLLC scenarios.

The main goal of this paper is to extend the framework

introduced in [15] to the case of cell-free Massive MIMO, and to use this framework to perform numerical experiments that shed light into the design of cell-free Massive MIMO architectures able to support URLLC traffic in UL and downlink (DL).

### A. State of the Art

Several attempts to account for finite-blocklength effects when characterizing the performance of cellular and cell-free Massive MIMO networks can be found in the literature. For example, the authors of [19], [20] assumed that the fading channel stays constant during the transmission of a codeword (the so-called quasi-static fading scenario) and used the outage capacity as asymptotic performance metric to characterize the performance of cellular Massive MIMO. As illustrated in [15], although the quasi-static fading scenario is relevant for URLLC, the infinite-blocklength assumption implicit in outage analyses may yield significantly incorrect estimates of the error probability. Another drawback resulting from the use of the outage-capacity framework is that it is generally not possible to account for the channel state information (CSI) acquisition overhead, which is, however, significant in the URLLC regime [21]. Indeed, quasi-static channels can be learned perfectly at the receiver in the asymptotic limit of large blocklength by simply transmitting a number of pilot symbols that grows sublinearly with the blocklength. The attempts made so far to include channel-estimation overhead in the outage setup [19], [20] are not convincing from a theoretical perspective, since they partly rely on results that hold only in the ergodic setting.

A theoretically satisfying framework that results in practically relevant information-theoretic upper bounds on the error probability was introduced in [15]. This framework encompasses the use of a mismatch receiver that treats the channel estimate, obtained using a fixed number of pilot symbols, as perfect, and it relies on the finite-blocklength tools developed in [16], [17] and later extended to wireless fading channels in, e.g., [21]–[23].

Finite-blocklength analyses have been recently conducted for both cellular Massive MIMO networks [24]–[26] and cell-free Massive MIMO networks [27]. The analysis in these papers relies on the so-called *normal approximation* [16, Eq. (291)], which, although capturing finite-blocklength effects, tends to suffer from low accuracy for the error probabilities that are of interest in URLLC [15]. Furthermore, the use of the normal approximation for the case of imperfect CSI in both [24] and [25] is not convincing, since the provided approximation does not depend on the instantaneous channel estimation error, but only on its variance. This is not compatible with a scenario in which the channel stays constant over the duration of each codeword. The analysis conducted in [27] is limited to the case in which perfect CSI is available at the receiver, which, as already mentioned, is not a reasonable assumption in the URLLC regime.

### B. Contributions

We present a general framework for characterizing in a numerical efficient way the packet error probability achiev-

able in cell-free Massive MIMO architectures supporting URLLC services. Our framework, which generalizes to cell-free Massive MIMO architectures the one presented in [15] for cellular Massive MIMO architectures, is applicable to both centralized and distributed cell-free systems, and allows for arbitrary fading distributions, channel estimation schemes, and spatial combining/precoding processing. We use the proposed framework to conduct numerical experiments pertaining an automated-factory deployment scenario, with the objective to compare the performance of cellular and cell-free Massive MIMO architectures and to draw guidelines for the design of cell-free architectures providing URLLC services. As performance metric, we use the network availability, which we define as the fraction of UE placements for which the per-link error probability, averaged over the small-scale fading and the additive noise, is below the URLLC target. The following conclusions can be drawn from our numerical experiments:

- (i) Minimum mean-square error (MMSE) spatial processing is necessary to achieve the URLLC reliability requirements, independently of the chosen architecture.
- (ii) For a fixed total number of antennas per coverage area, centralized cell-free architectures with single-antenna APs offer the best UL performance. Indeed, in the URLLC regime it is beneficial to minimize the average distance between UEs and APs by densifying the AP deployment. The use of multiple antennas at the APs is not beneficial, if it results in a reduction of the number of deployed APs.
- (iii) For this observation to apply to the DL as well, precoded DL pilots need to be transmitted by the APs to allow the UE to acquire channel knowledge. Without DL pilots, the DL performance of the centralized cell-free architecture degrades significantly, and becomes inferior to that of a distributed cell-free architecture with multiple-antenna APs.

We notice that the above conclusions also hold true in the ergodic regime when the average sum spectral efficiency of cell-free networks is considered. In this context, the first and second observations have been previously reported in, e.g., [13], [14] while the third one can be found in, e.g., [28]. Our numerical experiments not only confirm these previous findings but further reinforce them. For example, while in [13], [14] the MMSE processing was shown to be the preferable option for cell-free networks, our analysis shows that it is *mandatory* to satisfy the stringent requirements of URLLC scenarios. The same is valid for the use of downlink pilots.

### C. Paper Outline

In Section II, we present the proposed finite-blocklength framework, and we use it to illustrate, for a simple nonfading scenario, the benefits of cell-free architectures over cellular architectures for URLLC services. In Section III, we introduce a general finite-blocklength system model for cell-free Massive MIMO networks. This is used in Section IV to detail the UL and DL of different network architectures. The preliminary analysis reported in Section II is then extended to the more

practically relevant fading networks considered in Section V. Some conclusions are drawn in Section VI.

#### D. Notation

Lower-case bold letters are used for vectors and upper-case bold letters are used for matrices. The circularly-symmetric Gaussian distribution is denoted by  $\mathcal{CN}(0, \sigma^2)$ , where  $\sigma^2$  is its variance. We use  $\mathbb{E}[\cdot]$  to indicate the expectation operator,  $\mathbb{V}[\cdot]$  to indicate the variance operator, and  $\mathbb{P}[\cdot]$  for the probability of an event. The natural logarithm is denoted by  $\log(\cdot)$ , and  $Q(\cdot)$  stands for the Gaussian  $Q$ -function. The operators  $(\cdot)^T$ ,  $(\cdot)^*$ , and  $(\cdot)^H$  denote transpose, complex conjugate, and Hermitian transpose, respectively. The Euclidean norm is denoted by  $\|\cdot\|$ .

#### E. Reproducible Research

The Matlab code used to obtain the simulation results is available at: [https://github.com/infotheorychalmers/URLLC\\_cell-free\\_Massive\\_MIMO](https://github.com/infotheorychalmers/URLLC_cell-free_Massive_MIMO).

## II. REVIEW OF A FINITE-BLOCKLENGTH UPPER-BOUND ON THE ERROR PROBABILITY

### A. Desirable Features

A finite-blocklength information-theoretic framework to characterize the performance achievable in multiuser Massive MIMO systems, be them cellular or cell-free, needs to capture the following aspects:

- It must allow for linear spatial processing, used to separate the signals generated by/intended to the different UEs.
- It must allow for pilot-based CSI acquisition and apply to the practically relevant scenario in which decoding is performed under the assumption that the acquired CSI is exact.
- It must apply to a scenario in which the additive noise term includes not only thermal noise, but also residual multiuser interference after spatial processing.

We proceed as in [15] and start by considering the simple case in which the received signal is the superposition of a scaled version of the desired signal and additive Gaussian noise. We present a finite-blocklength upper bound on the error probability for this simplified channel model (Section II-B), and describe an efficient method for its numerical evaluation (Section II-C), based on the saddlepoint approximation [24, Ch. XVI]. The simple channel model introduced in this section constitutes the building block for the analysis of the error probability achievable in cell-free Massive MIMO networks. In Section II-D, we use the finite-blocklength bound, suitably adapted to cell-free networks, to exemplify the potential gains provided by cell-free architectures over cellular architectures on a simplified nonfading setup. This will motivate the more thorough studies performed in Section V. We emphasize that the finite-blocklength upper bound presented in Section II-B and its numerically efficient saddlepoint approximation presented in Section II-C coincide with the ones reported in [15]. However, their adaptation (see Sections III and IV) to both centralized and distributed cell-free architectures, as well as to

the case of precoded DL pilot transmission, is novel. Indeed, the analysis in [15] is limited to cellular Massive MIMO networks. Furthermore, even though precoded DL pilots have been considered in the literature (see, e.g., [28]), to the best of our knowledge, this is the first time they are considered in the context of short-packet communications.

### B. Random-coding union bound

A framework satisfying the requirements listed in Section II-A can be obtained via the so-called random-coding union bound with parameter  $s$  (RCUs) introduced in [17]. To introduce this bound, let us consider the following scalar input-output relation:

$$v[k] = gq[k] + z[k], \quad k = 1, \dots, n. \quad (1)$$

Here,  $q[k]$  denotes the  $k$ th entry of the length- $n$  codeword transmitted by a given user,  $v[k]$  is the corresponding received signal after linear processing,  $g$  denotes the effective channel after linear processing, which we assume to stay constant over the duration of the codeword, and  $z[k]$  is the additive noise signal, which includes also the residual multiuser interference. Note that, in this paper, we use the packet length  $n$  (also referred to as blocklength) as a proxy for the latency experienced in the access part of the wireless network. We do not model in our analysis delays due to user scheduling, nor the additional delays experienced in the transmission/processing of the information data over the fronthaul connecting the APs to the CPU.

To derive the bound, we shall assume that the receiver does not know  $g$ , but has access to an estimate  $\hat{g}$  that is treated as perfect. This estimate may be obtained via pilot transmission, or may simply be based on the knowledge of first-order statistics of  $g$ . The first situation is relevant in the UL, whereas the second situation typically occurs in the DL (see, e.g., [8]).

To estimate the transmitted codeword, the decoder performs scaled nearest-neighbor (SNN) decoding, i.e., it seeks the codeword that, after being scaled by the estimated channel gain  $\hat{g}$ , is closest to the received vector. Mathematically, the decoder solves the following problem:

$$\hat{\mathbf{q}} = \arg \min_{\mathbf{q} \in \mathcal{C}} \|\mathbf{v} - \hat{g}\mathbf{q}\|^2. \quad (2)$$

Here,  $\mathbf{v} = [v[1], \dots, v[n]]^T$ , the vector  $\hat{\mathbf{q}}$  stands for the codeword chosen by the decoder, and  $\mathcal{C}$  denotes the set of length- $n$  codewords.

The RCUs provides a random coding bound on the packet error probability  $\epsilon = \mathbb{P}[\hat{\mathbf{q}} \neq \mathbf{q}]$  achieved when the decoder operates according to the rule (2). The following theorem provides such a bound for the case of Gaussian codebooks, i.e., codebooks with codeword entries generated independently from a  $\mathcal{CN}(0, \rho)$  distribution.

*Theorem 1 ([15, Th. 1]):* Assume that  $g \in \mathbb{C}$  and  $\hat{g} \in \mathbb{C}$  in (1) are random variables drawn according to an arbitrary joint distribution. For all  $s > 0$ , there exists a coding scheme with  $m$  codewords of length  $n$  operating according to the

mismatched SNN decoding rule (2), whose error probability  $\epsilon$  is upper-bounded by

$$\begin{aligned} \epsilon &= \mathbb{P}[\hat{\mathbf{q}} \neq \mathbf{q}] \\ &\leq \mathbb{E}_{g, \hat{g}} \left[ \mathbb{P} \left[ \sum_{k=1}^n \iota_s(q[k], v[k]) \leq \log \frac{m-1}{u} \middle| g, \hat{g} \right] \right]. \end{aligned} \quad (3)$$

Here,  $u$  is a random variable that is uniformly distributed over the interval  $[0, 1]$  and  $\iota_s(q[k], v[k])$  is the so-called *generalized information density*, which for the case of Gaussian codebooks, is given by

$$\begin{aligned} \iota_s(q[k], v[k]) &= -s |v[k] - \hat{g}q[k]|^2 \\ &\quad + \frac{s|v[k]|^2}{1 + s\rho|\hat{g}|^2} + \log(1 + s\rho|\hat{g}|^2). \end{aligned} \quad (4)$$

Finally, the average in (3) is taken over the joint distribution of  $g$  and  $\hat{g}$ .

*Proof:* See [15, App. A]. ■

*Remark 1:* Note that the bound is valid for all values of  $s > 0$  and can be tightened by performing an optimization over this parameter. We also highlight that bound (3) holds for any channel law  $g$  and channel estimate  $\hat{g}$ . The implications of this property will become clear in Section IV. In (3), we used the law of total probability to express the RCUs as an average, over the channel  $g$  and its estimate  $\hat{g}$  of a tail probability. This will turn out convenient in view of the application of the saddlepoint method, discussed in the next section. Note that, although the tail probability is conditioned with respect to  $g$ , this does not mean that  $g$  is revealed to the receiver. Indeed, the operation performed by the receiver is fully specified by (2), which requires only knowledge of  $\hat{g}$ .

*Remark 2:* Within the context of point-to-point single-antenna transmission, the penalty incurred by the choice of using pilot-aided transmission instead of more sophisticated noncoherent schemes that do not require channel estimates was characterized in [21] using information-theoretic bounds similar to the ones used in this paper. As shown in [21], one attractive feature of the SNN decoder is that information-theoretic bounds on its error probability can be approached in practice using good channel codes for the nonfading AWGN channel. In contrast, for the optimal noncoherent ML decoder considered in, e.g., [29], approaching information-theoretic error-probability bounds with low-complexity coding schemes is still an open problem (note, however, the recent progress reported in [30]).

### C. Saddlepoint approximation

Unfortunately, the bound (3) is difficult to evaluate numerically. Indeed, the conditional probability inside the expectation in (3) is not known in closed form, and evaluating it accurately for the error-probabilities of interest in URLLC is time consuming. One common approach to simplify its evaluation is to invoke the Berry-Esseen central limit theorem [31, Ch. XVI.5] and replace the probability in (3) with a closed-form approximation that involves the Gaussian  $Q(\cdot)$  function and the first two moments of the generalized information

density, which can be expressed in closed form.<sup>1</sup> The resulting approximation is given as

$$\begin{aligned} \mathbb{P} \left[ \sum_{k=1}^n \iota_s(q[k], v[k]) \leq \log \frac{m-1}{u} \right] \\ = Q \left( \frac{nI_s - \log(m-1)}{\sqrt{nV_s}} \right) + \mathcal{O} \left( \frac{1}{\sqrt{n}} \right) \end{aligned} \quad (5)$$

where  $I_s = \mathbb{E}[\iota_s(q[1], v[1])]$  is the so-called *generalized mutual information* [32, Sec. III],

$$V_s = \mathbb{E}[\iota_s(q[1], v[1]) - I_s]^2 \quad (6)$$

is the variance of the information density, typically referred to as *channel dispersion* [16, Sec. IV], and  $\mathcal{O}(1/\sqrt{n})$  accounts for terms that decay no slower than  $1/\sqrt{n}$  as  $n \rightarrow \infty$ . Neglecting the  $\mathcal{O}(1/\sqrt{n})$  term in (5), we obtain the so-called *normal approximation*. As shown in [15, Fig. 1], this approximation is accurate only when the rate  $R = (\log m)/n$  is close to  $I_s$  [29], as a consequence of the central limit theorem [33, Ch. 5.11]. Unfortunately, this is typically not the case for the low error-probabilities of interest in URLLC.

An alternative approximation, which turns out to be accurate for a much larger range of error-probability values, including the ones of interest in URLLC, can be obtained using the so-called *saddlepoint method* [31, Ch. XVI]. The resulting approximation for the conditional probability inside the expectation in (3) is also in closed form for the setup considered in the present paper. As a consequence, the resulting approximation, commonly referred to as saddlepoint approximation, has essentially the same computational complexity as the normal approximation. A detailed analysis of the complexity and the accuracy of various types of normal and saddlepoint approximations was recently reported in [34]. For the setup considered in this section, the saddlepoint approximation was previously derived in [15, Th. 2]. We provide it in Theorem 2 below for completeness and emphasize that this is not a novel contribution of this paper.

*Theorem 2:* Let  $m = e^{nR}$  for some  $R > 0$ , and define  $\kappa(\zeta)$ ,  $\kappa'(\zeta)$  and  $\kappa''(\zeta)$  as

$$\begin{aligned} \kappa(\zeta) &= -\zeta \log(1 + s\rho|\hat{g}|^2) \\ &\quad - \log(1 + (\beta_B - \beta_A)\zeta - \beta_A\beta_B(1 - \nu)\zeta^2) \end{aligned} \quad (7)$$

$$\begin{aligned} \kappa'(\zeta) &= -\log(1 + s\rho|\hat{g}|^2) \\ &\quad - \frac{(\beta_B - \beta_A) - 2\beta_A\beta_B(1 - \nu)\zeta}{1 + (\beta_B - \beta_A)\zeta - \beta_A\beta_B(1 - \nu)\zeta^2} \end{aligned} \quad (8)$$

$$\begin{aligned} \kappa''(\zeta) &= \left[ \frac{(\beta_B - \beta_A) - 2\beta_A\beta_B(1 - \nu)\zeta}{1 + (\beta_B - \beta_A)\zeta - \beta_A\beta_B(1 - \nu)\zeta^2} \right]^2 \\ &\quad + \frac{2\beta_A\beta_B(1 - \nu)}{1 + (\beta_B - \beta_A)\zeta - \beta_A\beta_B(1 - \nu)\zeta^2} \end{aligned} \quad (9)$$

<sup>1</sup>Although to apply the Berry-Esseen theorem one needs to verify that the third absolute central moment is bounded, to evaluate the normal approximation one needs only to compute the first two moments, since the term involving the third absolute central moment is hidden in the  $\mathcal{O}(1/\sqrt{n})$  term in (5).



where

$$\beta_A = s(\rho|g - \hat{g}|^2 + \sigma^2) \quad (10)$$

$$\beta_B = \frac{s}{1 + s\rho|\hat{g}|^2}(\rho|g|^2 + \sigma^2) \quad (11)$$

$$\nu = \frac{s^2|\rho|g|^2 + \sigma^2 - g^*\hat{g}\rho}{\beta_A\beta_B(1 + s\rho|\hat{g}|^2)}. \quad (12)$$

One can show that  $I_s = -\kappa'(0)$ . Let  $R_s^{\text{cr}} = -\kappa'(1)$  and let  $\zeta \in (\zeta, \bar{\zeta})$  be the solution to the equation  $R = -\kappa'(\zeta)$ . If  $\zeta \in [0, 1]$ , then

$$\begin{aligned} \mathbb{P}\left[\sum_{k=1}^n \iota_s(q[k], v[k]) \leq \log \frac{e^{nR} - 1}{u}\right] \\ = e^{n[\kappa(\zeta) + \zeta R]} \left[ \Psi_{n,\zeta}(\zeta) + \Psi_{n,\zeta}(1 - \zeta) + o\left(\frac{1}{\sqrt{n}}\right) \right] \end{aligned} \quad (13)$$

where

$$\Psi_{n,\zeta}(u) \triangleq e^{n\frac{u}{2}\kappa''(\zeta)} Q\left(u\sqrt{n\kappa''(\zeta)}\right) \quad (14)$$

and  $o(1/\sqrt{n})$  comprises terms that vanish faster than  $1/\sqrt{n}$  and are uniform in  $\zeta$ . If  $\zeta > 1$ , then

$$\begin{aligned} \mathbb{P}\left[\sum_{k=1}^n \iota_s(q[k], v[k]) \leq \log \frac{e^{nR} - 1}{u}\right] \\ = e^{n[\kappa(1) + R]} \left[ \tilde{\Psi}_n(1, 1) + \tilde{\Psi}_n(0, -1) + \mathcal{O}\left(\frac{1}{\sqrt{n}}\right) \right] \end{aligned} \quad (15)$$

where

$$\begin{aligned} \tilde{\Psi}_n(a_1, a_2) \\ = e^{na_1[R_s^{\text{cr}} - R + \frac{\kappa''(1)}{2}]} Q\left(a_1\sqrt{n\kappa''(1)} + a_2\frac{n(R_s^{\text{cr}} - R)}{\sqrt{n\kappa''(1)}}\right) \end{aligned} \quad (16)$$

and  $\mathcal{O}(1/\sqrt{n})$  comprises terms that decay no slower than  $1/\sqrt{n}$  and are uniform in  $\zeta$ . If  $\zeta < 0$ , then

$$\begin{aligned} \mathbb{P}\left[\sum_{k=1}^n \iota_s(q[k], v[k]) \leq \log \frac{e^{nR} - 1}{u}\right] \\ = 1 - e^{n[\kappa(\zeta) + \zeta R]} \left[ \Psi_{n,\zeta}(-\zeta) - \Psi_{n,\zeta}(1 - \zeta) + o\left(\frac{1}{\sqrt{n}}\right) \right]. \end{aligned} \quad (17)$$

#### D. The benefit of cell-free networks over cellular networks in the finite-blocklength regime

We now use the bound in (3) together with the saddlepoint approximation from Theorem 2 to exemplify the benefits of cell-free networks over conventional cellular networks, in the URLLC regime. Following [14, Sec. 1.3], we compare three setups. The first one is a single cell with a 64-antenna Massive MIMO AP; the second one consists of 64 small cells served each by a single-antenna AP, deployed on a square grid; the last one is a cell-free network where the same 64 AP locations are used. In the small-cell network, each UE is associated to the AP providing the best performance. We focus on the UL and assume that  $K$  UEs are active in the coverage area. We

denote by  $\mathbf{h}_k = [h_{k1}, \dots, h_{kM}]^T \in \mathbb{C}^M$  the channel between UE  $k$  and the  $M = 64$  antennas or APs. The channel gain  $\beta(d_{kl})$  (i.e., pathloss or large-scale fading coefficient) for a propagation distance  $d_{kl}$  is modelled as [14, Sec. 1.3]

$$\beta(d) \text{ [dB]} = -30.5 - 36.7 \log_{10}\left(\frac{d}{1 \text{ m}}\right). \quad (18)$$

All channels are deterministic (i.e., no fading) and perfectly known to the APs. Detection is performed by using MMSE and maximum ratio (MR) combiners in all the three setups. Since no fading is present, no averaging over  $g$  and  $\hat{g}$  in (3) is required and the tail probability can be approximated efficiently using the saddlepoint approximations provided in Theorem 2.

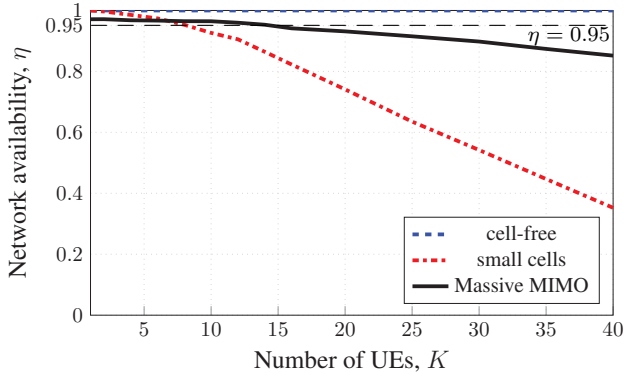
We consider a total coverage area of  $150 \text{ m} \times 150 \text{ m}$  and drop UEs uniformly at random in the area. We assume that the APs are deployed 10 m above the UEs. The noise power is  $-96$  dBm, which is a reasonable value when the bandwidth is 20 MHz. We consider a codeword length  $n = 100$  and a rate of  $R = 60/100 = 0.6$  bits per channel use.

The three different network setups are compared in terms of *network availability*,  $\eta$ . Following [15], this is defined as the probability, computed with respect to the random UEs' positions, that the error probability is below a given target  $\epsilon_{\text{target}}$ , i.e.,

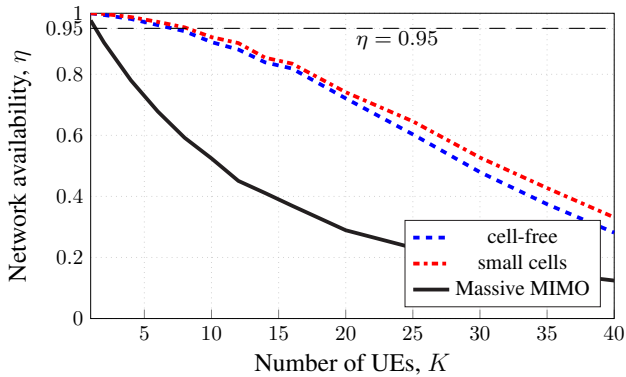
$$\eta = \mathbb{P}[\epsilon \leq \epsilon_{\text{target}}]. \quad (19)$$

Fig. 1 shows  $\eta$  for  $\epsilon_{\text{target}} = 10^{-5}$  as a function of the number of UEs  $K \in \{1, \dots, 40\}$ . The transmit power of each UE is  $\rho = -10$  dBm. We see that, with MMSE combiner (Fig. 1a), the cell-free network yields  $\eta = 1$  irrespective of  $K$ . This is not the case with small cells and Massive MIMO. Specifically, the small-cell network yields  $\eta = 1$  only when  $K = 1$ . When  $K = 20$ , the network availability decreases to approximately 0.75, and it further decreases to 0.35 when  $K = 40$ . Assume now that we are interested in achieving a network availability of 0.95 (indicated in the figures by a dashed line). This value of  $\eta$  is achievable with small cells only when  $K \leq 7$ . The cell-free network performs better than small cells because of its superior ability in managing interference. Note that Massive MIMO cannot achieve  $\eta = 1$  even when  $K = 1$ . This is due to the larger maximum distance between a randomly placed UE and the BS. Furthermore, the performance of Massive MIMO decreases, although only marginally, compared to the small-cell case, as  $K$  increases. With the MR combiner (Fig. 1b), a network availability  $\eta \geq 0.95$  is reached by the cell-free network and by the small-cell network when  $K \leq 7$ , and cannot be achieved by the Massive MIMO network even when  $K = 1$ . Perhaps surprisingly, the small-cell network slightly outperforms the cell-free network, which implies that cooperation is only beneficial when the interference is properly managed via the use of an MMSE combiner.

In Fig. 2, we plot  $\eta$  as a function of the transmit power  $\rho \in \{-20, \dots, 20\}$  dBm,  $\epsilon_{\text{target}} = 10^{-5}$  and  $K = 10$ . With the MMSE combiner (Fig. 2a), cell-free yields  $\eta$  close to 1 irrespective of  $\rho$ . On the contrary, this is possible with Massive MIMO only when  $\rho \geq -8$  dBm. A small-cell network performs better than Massive MIMO for  $\rho \leq -11$  dBm, but



(a) With MMSE combiner

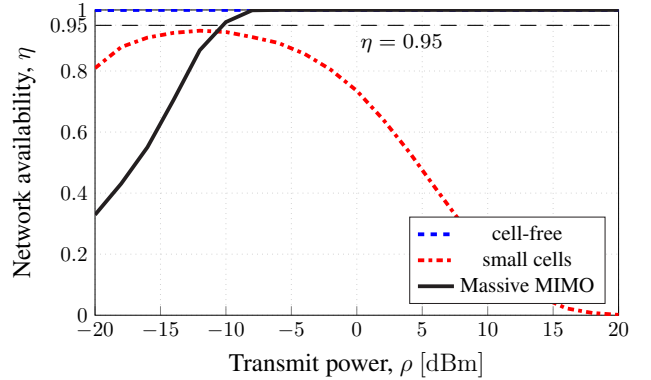


(b) With MR combiner

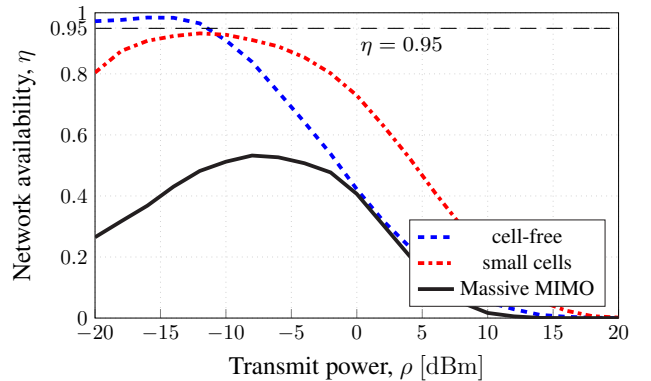
Fig. 1: Network availability for each of the three network configurations as a function of the number of active UEs. The total number of antennas or APs is 64 in all network configurations and the transmit power of each UE is  $\rho = -15$  dBm.

its network availability vanishes as  $\rho$  increases and does not achieve  $\eta \geq 0.95$ . Indeed, as the transmit power increases, so does the intercell interference, which rapidly prevents the network from achieving the target error probability. With the MR combiner (Fig. 2b), a network availability above 0.95 can be only achieved by the cell-free network when  $\rho \leq -11$  dBm, and it cannot be achieved with Massive MIMO or small cells. Again, the small-cell network outperforms the cell-free network as the transmit power grows. This confirms once more the importance of effective interference management via the use of MMSE spatial processing in order to benefit from AP cooperation.

To summarize, from the above analysis, we can conclude that the cell-free architecture is vastly superior to Massive MIMO and small cells in providing high network availability for the packet error probabilities of interest in URLLC. However, some strong assumptions were made in the analysis: nonfading channels, perfect channel state information, and full cooperation among the APs. The question thus is: *Can high network availability be achieved in the UL and DL of practical (centralized or decentralized) cell-free networks where these assumptions are typically not met?*



(a) With MMSE combiner



(b) With MR combiner

Fig. 2: Network availability for each of the three network configurations as a function of the transmit power of each UE. The total number of antennas or APs is 64 and the number of UEs is  $K = 10$ .

### III. CELL-FREE NETWORK MODEL

To answer the above question, we now present a more refined system model, which will allow us to generalize the observations reported in Section II-D to more practically relevant scenarios. Specifically, we consider a cell-free Massive MIMO network with  $L$  APs, each equipped with  $M$  antennas, which are geographically distributed over the coverage area. The APs serve jointly  $K$  single-antenna UEs, and are connected via fronthaul links to the CPU. The standard time-division duplexing protocol of cellular Massive MIMO is used, where the  $n$  available channel uses are divided as follows:  $n_p^{\text{ul}}$  symbols for UL pilots;  $n^{\text{ul}}$  symbols for UL data;  $n_p^{\text{dl}}$  symbols for DL pilots; and  $n^{\text{dl}}$  symbols for DL data. Note that we explicitly allow in our system model for the use of precoded downlink pilots. In URLLC scenarios, their presence will turn out critical to achieve high network availability in the DL.

The channel between AP  $l$  and UE  $i$  is denoted by  $\mathbf{h}_{il} \in \mathbb{C}^M$ . We use a correlated Rayleigh fading model where  $\mathbf{h}_{il} \sim \mathcal{CN}(\mathbf{0}_M, \mathbf{R}_{il})$  remains constant for the duration of the  $n$  channel uses. The normalized trace  $\beta_{il} = \text{tr}(\mathbf{R}_{il})/M$  determines the average large-scale fading between AP  $l$  and UE  $i$ , while the eigenstructure of  $\mathbf{R}_{il}$  describes its spatial channel correlation [8, Sec. 2.2]. We assume that the channel vectors of different APs are independently distributed; thus  $\mathbb{E}\{\mathbf{h}_{il}\mathbf{h}_{il'}^H\} = \mathbf{0}_{ML}$ , for  $l \neq l'$ . This is a reasonable

assumption because the APs are typically separated by tens of wavelengths or more. The collective channel vector  $\mathbf{h}_i = [\mathbf{h}_{i1}^T \dots \mathbf{h}_{iL}^T]^T \in \mathbb{C}^{ML}$  follows a  $\mathcal{CN}(\mathbf{0}_{ML}, \mathbf{R}_i)$  distribution, where  $\mathbf{R}_i = \text{diag}(\mathbf{R}_{i1}, \dots, \mathbf{R}_{iL})$ . We assume that the spatial correlation matrices  $\mathbf{R}_{il}$  are known to the CPU in a centralized implementation, while each AP has access to its local spatial correlation matrices in a distributed implementation. See, e.g., [9, Sec. IV] for practical methods for estimating spatial correlation matrices.

### A. Uplink and Downlink Data Transmission

In the UL, we denote by  $x_i^{\text{ul}}[k]$  the signal transmitted by UE  $i$  over channel use  $k$ . The received complex baseband signal  $\mathbf{r}_l^{\text{ul}}[k] \in \mathbb{C}^M$  at AP  $l$  and channel use  $k \in \{1, \dots, n^{\text{ul}}\}$  is given by

$$\mathbf{r}_l^{\text{ul}}[k] = \sum_{i=1}^K \mathbf{h}_{il} x_i^{\text{ul}}[k] + \mathbf{z}_l^{\text{ul}}[k] \quad (20)$$

where  $\mathbf{z}_l^{\text{ul}}[k]$  denotes the noise vector at AP  $l$ , which contains i.i.d. entries, distributed according to  $\mathcal{CN}(0, \sigma_{\text{ul}}^2)$ .

Similarly, in the DL we denote by  $x_i^{\text{dl}}[k]$  the signal intended for UE  $i$  over channel use  $k \in \{1, \dots, n^{\text{dl}}\}$ . Let  $\mathbf{w}_{il} \in \mathbb{C}^M$  denote the precoder that AP  $l$  assigns to UE  $i$ . In the DL, the received signal at UE  $i$  over channel use  $k$  is

$$y_i^{\text{dl}}[k] = \sum_{l=1}^L \mathbf{h}_i^H \sum_{j=1}^K \mathbf{w}_{jl} x_j^{\text{dl}}[k] + z_i^{\text{dl}}[k] \quad (21)$$

$$= \mathbf{h}_i^H \mathbf{w}_i x_i^{\text{dl}}[k] + \mathbf{h}_i^H \sum_{j=1, j \neq i}^K \mathbf{w}_j x_j^{\text{dl}}[k] + z_i^{\text{dl}}[k] \quad (22)$$

where  $\mathbf{w}_i = [\mathbf{w}_{i1}^T \dots \mathbf{w}_{iL}^T]^T \in \mathbb{C}^{ML}$  is the collective precoding vector, and  $z_i^{\text{dl}}[k] \sim \mathcal{CN}(0, \sigma_{\text{dl}}^2)$  is the noise at UE  $i$ . Note also that the precoded channel  $\mathbf{h}_i^H \mathbf{w}_i$  is not Rayleigh distributed. As we remarked in Section II-B, this is not a problem since the bound (3) holds for any channel law  $g$  and channel estimate  $\hat{g}$ .

### B. Uplink Pilot Transmission and Channel Estimation

The UL pilot signature of UE  $i$  is denoted by the vector  $\phi_i \in \mathbb{C}^{n_p^{\text{ul}}}$  satisfying  $\|\phi_i\|^2 = n_p^{\text{ul}}$ . The elements of  $\phi_i$  are scaled by the square-root of the pilot power  $\sqrt{\rho^{\text{ul}}}$  and transmitted over  $n_p^{\text{ul}}$  channel uses. At AP  $l$ , the received pilot signal  $\mathbf{Y}_l^{\text{pilot}} \in \mathbb{C}^{M \times n_p^{\text{ul}}}$  is

$$\mathbf{Y}_l^{\text{pilot}} = \sqrt{\rho^{\text{ul}}} \sum_{i=1}^K \mathbf{h}_{il} \phi_i^H + \mathbf{Z}_l^{\text{pilot}} \quad (23)$$

where  $\mathbf{Z}_l^{\text{pilot}} \in \mathbb{C}^{M \times n_p^{\text{ul}}}$  is noise with independent  $\mathcal{CN}(0, \sigma_{\text{ul}}^2)$ -distributed elements. Since the CPU has access to the covariance matrices  $\{\mathbf{R}_{il}\}$ , it can compute the MMSE estimate of  $\mathbf{h}_{il}$  as [8, Sec. 3.2]

$$\hat{\mathbf{h}}_{il} = \sqrt{\rho^{\text{ul}}} \mathbf{R}_{il} \mathbf{Q}_{il}^{-1} \left( \mathbf{Y}_l^{\text{pilot}} \phi_i \right) \quad (24)$$

with  $\mathbf{Q}_{il} = \rho^{\text{ul}} \sum_{i'=1}^K \mathbf{R}_{il} \phi_{i'}^H \phi_{i'} + \sigma_{\text{ul}}^2 \mathbf{I}_M$ . We let  $\hat{\mathbf{h}}_i = [\hat{\mathbf{h}}_{i1}^T \dots \hat{\mathbf{h}}_{iL}^T]^T$ . The estimation error is  $\mathbf{h}_i - \hat{\mathbf{h}}_i \sim \mathcal{CN}(\mathbf{0}, \mathbf{C}_i)$  with  $\mathbf{C}_i = \mathbf{R}_i - \Phi_i$  and  $\Phi_i = \text{diag}(\Phi_{i1}, \dots, \Phi_{iL})$ , where  $\Phi_{il} = \rho^{\text{ul}} n_p \mathbf{R}_{il} \mathbf{Q}_{il}^{-1} \mathbf{R}_{il}$ .

### C. Downlink Pilot Transmission and Channel Estimation

As in the UL, we denote the DL pilot signature assigned to UE  $i$  by the vector  $\phi_i \in \mathbb{C}^{n_p^{\text{dl}}}$  satisfying  $\|\phi_i\|^2 = n_p^{\text{dl}}$ . The elements of  $\phi_i$  are scaled by the square-root of the DL pilot power  $\sqrt{\rho^{\text{dl}}}$  and transmitted over  $n_p^{\text{dl}}$  channel uses. It follows from (22), that the received signal  $\mathbf{y}_i^{\text{pilot}} \in \mathbb{C}^{1 \times n_p^{\text{dl}}}$  at UE  $i$  is

$$\begin{aligned} \mathbf{y}_i^{\text{pilot}} &= \sqrt{\rho^{\text{dl}}} \mathbf{h}_i^H \sum_{j=1}^K \mathbf{w}_j \phi_j^H + \mathbf{z}_i^{\text{pilot}} \\ &= \sqrt{\rho^{\text{dl}}} \xi_{ii} \phi_i^H + \sqrt{\rho^{\text{dl}}} \sum_{j=1, j \neq i}^K \xi_{ij} \phi_j^H + \mathbf{z}_i^{\text{pilot}} \end{aligned} \quad (25)$$

where  $\xi_{ij} = \mathbf{h}_i^H \mathbf{w}_j$  denotes the effective precoded channel to UE  $i$  and  $\mathbf{z}_i^{\text{pilot}} \in \mathbb{C}^{1 \times n_p^{\text{dl}}}$  is noise with independent  $\mathcal{CN}(0, \sigma_{\text{dl}}^2)$ -distributed elements. The UE multiplies the received row vector  $\mathbf{y}_i^{\text{pilot}}$  with its pilot signature to obtain

$$\tilde{y}_i = \mathbf{y}_i^{\text{pilot}} \phi_i = \sqrt{\rho^{\text{dl}}} n_p^{\text{dl}} \xi_{ii} + \tilde{z}_i \quad (26)$$

with

$$\tilde{z}_i = \sqrt{\rho^{\text{dl}}} \sum_{j=1, j \neq i}^K \xi_{ij} \phi_j^H \phi_i + \mathbf{z}_i^{\text{pilot}} \phi_i. \quad (27)$$

Since  $\xi_{ii}$  is in general not Gaussian distributed, the MMSE channel estimator cannot be expressed in closed form. If both the mean and the variance of  $\xi_{ii}$  are known, one can utilize the LMMSE estimator, which is given by [8, App. B.4]

$$\begin{aligned} \hat{\xi}_{ii} &= \mathbb{E}[\xi_{ii}] + \frac{\sqrt{\rho^{\text{dl}}} n_p^{\text{dl}} \mathbb{V}[\xi_{ii}]}{\rho^{\text{dl}} (n_p^{\text{dl}})^2 \mathbb{V}[\xi_{ii}] + \mathbb{V}[\tilde{z}_i]} \\ &\quad \times \left( \tilde{y}_i - \sqrt{\rho^{\text{dl}}} n_p^{\text{dl}} \mathbb{E}[\xi_{ii}] - \mathbb{E}[\tilde{z}_i] \right). \end{aligned} \quad (28)$$

An alternative approach is to use the least-squares (LS) estimator, which yields

$$\hat{\xi}_{ii} = \frac{1}{\sqrt{\rho^{\text{dl}}} n_p^{\text{dl}}} \tilde{y}_i. \quad (29)$$

Unlike the LMMSE estimator, the LS estimator does not require the knowledge of the statistics (i.e., mean and variance) of the precoded channel  $\xi_{ii}$ , and thus is easier to implement. A similar precoded DL pilot scheme was considered in [28] in the context of spectral efficiency analyses of cell-free networks. Differently from our analysis, however, the one performed in [28] considers only distributed cell-free networks, MR precoding, and LMMSE channel estimation.

## IV. UPLINK AND DOWNLINK OPERATION

We now detail the UL and DL of two different implementations of cell-free Massive MIMO, namely, centralized and distributed.

### A. Uplink

1) *Centralized Operation:* In the UL of a fully centralized implementation, each AP  $l$  acts only as a remote-radio head, i.e., as a relay that forwards its received baseband signal  $\mathbf{r}_l^{\text{ul}}[k]$  to the CPU, which performs channel estimation and data detection after linear processing. Specifically, to decode the signal from UE  $i$ , the CPU computes for  $k = 1, \dots, n^{\text{ul}}$

$$\mathbf{y}_i^{\text{ul}}[k] = \mathbf{u}_i^{\text{H}} \mathbf{r}^{\text{ul}}[k] \quad (30)$$

where  $\mathbf{u}_i = [\mathbf{u}_{i1}^{\text{T}} \dots \mathbf{u}_{iL}^{\text{T}}]^{\text{T}} \in \mathbb{C}^{ML}$  is the centralized linear-combining vector and  $\mathbf{r}^{\text{ul}}[k] \in \mathbb{C}^{ML}$  is the collective UL data signal, given by

$$\mathbf{r}^{\text{ul}}[k] = \begin{bmatrix} \mathbf{r}_1^{\text{ul}}[k] \\ \vdots \\ \mathbf{r}_L^{\text{ul}}[k] \end{bmatrix} = \sum_{i=1}^K \mathbf{h}_i x_i^{\text{ul}}[k] + \mathbf{z}^{\text{ul}}[k] \quad (31)$$

with  $\mathbf{z}^{\text{ul}}[k] = [\mathbf{z}_1^{\text{ulT}}[k] \dots \mathbf{z}_L^{\text{ulT}}[k]]^{\text{T}} \in \mathbb{C}^{ML}$  being the collective noise vector. Substituting (30) into (31) we obtain

$$\mathbf{y}_i^{\text{ul}}[k] = \underbrace{\mathbf{u}_i^{\text{H}} \mathbf{h}_i}_{g} \underbrace{x_i^{\text{ul}}[k]}_{q[k]} + \underbrace{\sum_{j=1, j \neq i}^K \mathbf{u}_i^{\text{H}} \mathbf{h}_j x_j^{\text{ul}}[k] + \mathbf{u}_i^{\text{H}} \mathbf{z}^{\text{ul}}[k]}_{z[k]} \quad (32)$$

which can be expressed in the same form as (1) if we set  $v[k] = y_i^{\text{ul}}[k]$ ,  $q[k] = x_i^{\text{ul}}[k]$ ,  $g = \mathbf{u}_i^{\text{H}} \mathbf{h}_i$ , and  $z[k] = \sum_{j=1, j \neq i}^K \mathbf{u}_i^{\text{H}} \mathbf{h}_j x_j^{\text{ul}}[k] + \mathbf{u}_i^{\text{H}} \mathbf{z}^{\text{ul}}[k]$ . Given all channels and combining vectors, the random variables  $\{z[k] : k = 1, \dots, n^{\text{ul}}\}$  are conditionally i.i.d. and  $z[k] \sim \mathcal{CN}(0, \sigma^2)$  with  $\sigma^2 = \sigma_{\text{ul}}^2 \|\mathbf{u}_i\|^2 + \rho^{\text{ul}} \sum_{j=1, j \neq i}^K |\mathbf{u}_i^{\text{H}} \mathbf{h}_j|^2$ .

We assume that the CPU treats the channel estimate  $\hat{\mathbf{h}}_i$  as perfect and that the transmitted codeword is drawn from a codebook  $\mathcal{C}^{\text{ul}}$ . The estimated codeword  $\hat{\mathbf{x}}_i^{\text{ul}}$  is thus obtained by performing mismatched SNN decoding with  $\hat{g} = \mathbf{u}_i^{\text{H}} \hat{\mathbf{h}}_i$ , i.e.,

$$\hat{\mathbf{x}}_i^{\text{ul}} = \arg \min_{\hat{\mathbf{x}}_i^{\text{ul}} \in \mathcal{C}^{\text{ul}}} \|\mathbf{y}_i^{\text{ul}} - \hat{g} \hat{\mathbf{x}}_i^{\text{ul}}\|^2 \quad (33)$$

with  $\mathbf{y}_i^{\text{ul}} = [y_i^{\text{ul}}[1], \dots, y_i^{\text{ul}}[n^{\text{ul}}]]^{\text{T}}$  and  $\hat{\mathbf{x}}_i^{\text{ul}} = [\hat{x}_i^{\text{ul}}[1], \dots, \hat{x}_i^{\text{ul}}[n^{\text{ul}}]]^{\text{T}}$ . An upper bound on the packet error probability then follows by applying (3). It is important to note that, although we assumed Rayleigh fading and MMSE channel estimation, the obtained bound is actually valid for any channel law and channel-estimation method, as well as any choice of the spatial combiner  $\mathbf{u}_i$ . For a detailed discussion on centralized combining schemes, we refer the interested reader to [14, Sec. 5.1.3, Sec. 5.1.4].

2) *Distributed Operation:* In a distributed cell-free network, the channel estimates are computed locally at the APs and are used to obtain local estimates of UE data. Hence, unlike a fully centralized network, AP  $l$  can only use its own local channel estimates for the design of the local combiner  $\mathbf{u}_{il}$ . The locally spatially-filtered signals at each AP are then sent to the CPU, which performs detection. We assume that the received signal at the CPU is the average of the locally filtered signals, i.e.,

$$\mathbf{y}_i^{\text{ul}}[k] = \sum_{l=1}^L \mathbf{u}_{il}^{\text{H}} \mathbf{r}_l^{\text{ul}}[k]. \quad (34)$$

In a distributed network, the CPU does not have knowledge of channel estimates and thus only the statistics can be utilized for data detection. Specifically, we assume that  $\hat{\mathbf{x}}_i^{\text{ul}}$  is obtained as in (33) but with

$$\hat{g} = \mathbb{E}[\mathbf{u}_i^{\text{H}} \mathbf{h}_i] = \sum_{l=1}^L \mathbb{E}[\mathbf{u}_{il}^{\text{H}} \mathbf{h}_{il}]. \quad (35)$$

As in the centralized case, the upper bound on the error probability, obtained from (3), is valid for any fading-channel distribution and any channel-estimation method as well as for any choice of local combiners  $\{\mathbf{u}_{il} : l = 1, \dots, L\}$ . For a detailed discussion on the choice of combiners, we refer the interested reader to [14, Sec. 6.1.2].

### B. Downlink Operation

We now consider the DL counterparts of the two UL operations described above.

1) *Centralized Operation:* In a centralized network, the CPU exploits channel reciprocity to obtain estimates of the collective channel vectors, which are then used to compute the precoding vectors. We assume that

$$\mathbf{w}_i = \sqrt{\rho_i^{\text{dl}}} \bar{\mathbf{w}}_i \quad (36)$$

where  $\|\bar{\mathbf{w}}_i\|^2 = 1$  so that  $\rho_i^{\text{dl}}$  can be thought as the DL transmit power. Different precoders yield different tradeoffs between the error probability achievable at the UEs. A common heuristic comes from UL-DL duality [8, Sec. 4.3.2], which suggests to choose the precoding vectors  $\mathbf{w}_i$  as the following function of the combining vectors:  $\mathbf{w}_i = \mathbf{u}_i / \sqrt{\mathbb{E}[\|\mathbf{u}_i\|^2]}$ .

As in UL, we can put (22) in the same form as (1) by setting  $v[k] = y_i^{\text{dl}}[k]$ ,  $q[k] = x_i^{\text{dl}}[k]$ ,  $g = \mathbf{h}_i^{\text{H}} \mathbf{w}_i$ , and  $z[k] = \sum_{j=1, i \neq j}^K \mathbf{h}_i^{\text{H}} \mathbf{w}_j x_j^{\text{dl}}[k] + z_i^{\text{dl}}[k]$ . The random variables  $\{z[k] : k = 1, \dots, n^{\text{dl}}\}$  are i.i.d. with  $z[k] \sim \mathcal{CN}(0, \sigma^2)$  and  $\sigma^2 = \sigma_{\text{dl}}^2 + \rho^{\text{dl}} \sum_{i'=1, i \neq i'}^K |\mathbf{h}_i^{\text{H}} \mathbf{w}_{i'}|^2$ . The estimated codeword is thus obtained by performing mismatched SNN decoding as

$$\hat{\mathbf{x}}_i^{\text{dl}} = \arg \min_{\hat{\mathbf{x}}_i^{\text{dl}} \in \mathcal{C}^{\text{dl}}} \|\mathbf{y}_i^{\text{dl}} - \hat{g} \hat{\mathbf{x}}_i^{\text{dl}}\|^2 \quad (37)$$

with  $\mathbf{y}_i^{\text{dl}} = [y_i^{\text{dl}}[1], \dots, y_i^{\text{dl}}[n^{\text{dl}}]]^{\text{T}}$  and  $\hat{\mathbf{x}}_i^{\text{dl}} = [\hat{x}_i^{\text{dl}}[1], \dots, \hat{x}_i^{\text{dl}}[n^{\text{dl}}]]^{\text{T}}$ .

Note that without pilot transmission in the DL, the UE has no knowledge of the precoded channel  $\xi_{ii} = \mathbf{h}_i^{\text{H}} \mathbf{w}_i$  in (22). We assume, however, that the UE is aware of its expected value  $\mathbb{E}[\mathbf{h}_i^{\text{H}} \mathbf{w}_i]$  and uses this quantity to perform mismatched SNN decoding. Specifically, we set  $\hat{g} = \mathbb{E}[\mathbf{h}_i^{\text{H}} \mathbf{w}_i]$  in (37). When pilots are transmitted in the DL, mismatched SNN decoding is performed with  $\hat{g} = \hat{\xi}_{ii}$  where  $\hat{\xi}_{ii}$  is computed using, e.g., the LS estimator (29).

2) *Distributed Operation:* We assume that the CPU produces the downlink codewords  $\{\mathbf{x}_i^{\text{dl}} : i = 1, \dots, K\}$  and send them to the serving APs. Each AP then performs spatial precoding on the basis of the available local channel estimates. For example the signal transmitted by AP  $l$  in channel use  $k$  is given by

$$\sum_{i=1}^K \mathbf{w}_{il} x_i^{\text{dl}}[k]. \quad (38)$$



TABLE I: Network parameters.

Parameter	Value
Network area	150 m × 150 m
Number of UEs	$K = 40$
Bandwidth	$B = 20$ MHz
Receiver noise power	$\sigma_{ul}^2 = \sigma_{dl}^2 = -96$ dBm
Number of information bits	$b = \log_2 m = 160$
Total number of channel uses	$n = 300$
Number of UL/DL channel uses	$n/2 = 150$
Number of UL pilots	$n_p^{ul} = 40$
Number of DL pilots	$n_p^{dl} = 0$ or $40$
Distance between UE $i$ and AP $l$	$d_{il}$
Large scale fading $\beta_{il}$ in dB	$-30.5 - 37.6 \log_{10} \left( \frac{d_{il}}{1\text{m}} \right)$
Height difference between AP and UE	10 m
Target error probability	$\epsilon_{\text{target}} = 10^{-5}$
Combining/precoding scheme	MMSE or MR

As in the centralized case, UE  $i$  detects the transmitted codeword by performing the mismatched SNN decoding operation in (37). Specifically, if no DL pilots are transmitted, the UE  $i$  sets  $\hat{g} = \mathbb{E}[\mathbf{h}_i^H \mathbf{w}_i]$ . If DL pilots are transmitted, UE  $i$  sets  $\hat{g} = \hat{\xi}_{ii}$ .

## V. NUMERICAL ANALYSIS

We present numerical simulations to characterize the UL and DL performance of the different cell-free Massive MIMO implementations in the URLLC regime. We consider an automated-factory propagation scenario with no wrap-around topology. The URLLC requirements for our numerical experiments, which are provided in Table I, have been selected according to the 3GPP technical specifications [2]. The number of UL and DL channel uses corresponds roughly to a resource block in 5G NR and yields a latency of around 100  $\mu$ s. When multiple antennas are used at the APs, the spatial correlation matrices are generated using the local scattering model from [8, Sec. 2.6]. Specifically, we assume that the scatterers are uniformly distributed in the angular interval  $[\varphi_i - \Delta, \varphi_i + \Delta]$ , where  $\varphi_i$  is the nominal angle-of-arrival of UE  $i$ , where  $i = 1, \dots, K$ , and  $\Delta$  is the angular spread. Hence, the  $(m_1, m_2)$ th element of  $\mathbf{R}_{il}$  is equal to [8, Sec. 2.6]

$$[\mathbf{R}_{il}]_{m_1, m_2} = \frac{\beta_{il}}{2\Delta} \int_{-\Delta}^{\Delta} e^{j\pi(m_1 - m_2) \sin(\varphi_i + \bar{\varphi})} d\bar{\varphi}. \quad (39)$$

In all subsequent simulations, we assume  $\Delta = 25^\circ$ .

The analysis is carried out by using the network availability  $\eta$  defined in (19) as performance metric. Specifically, for fixed UE positions, we compute the average UL and DL error probabilities  $\epsilon^{ul}$  and  $\epsilon^{dl}$  for an arbitrary UE within the coverage area by averaging over the small-scale fading and the additive noise. Then, we evaluate the probability, computed with respect to the random user positions, that  $\epsilon^{ul}$  or  $\epsilon^{dl}$  are below  $\epsilon_{\text{target}} = 10^{-5}$ . Similar to Section II-D, the use of MMSE combining and precoding in both the UL and the DL turns out to be mandatory to achieve high  $\eta$ . Hence, we will focus on MMSE combining and precoding in the remainder of the section.

When considering network architectures involving multiple APs, we assume that the APs are located on a square grid within the coverage area. This implies that the number  $L$  of

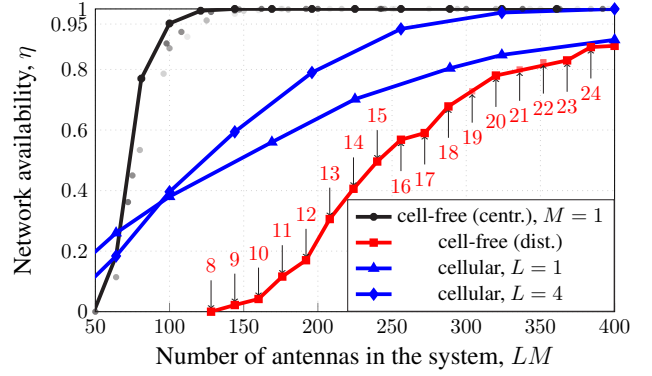


Fig. 3: UL network availability  $\eta$  with different network deployments as a function of  $LM$ . The labels indicate the number of AP antennas  $M$  that result in the largest  $\eta$  for the cell-free distributed case.

APs is chosen so that  $\sqrt{L}$  is an integer. When considering cell-free architectures, we will also assume that  $L \geq 16$ .

To perform a fair comparison, we use the same propagation model for cellular and cell-free simulations. Furthermore, the same UE locations and pilot assignments are used in both scenarios. We assume that the cellular BSs are equipped with half-wavelength-spaced uniform linear arrays. The spatial correlation follows the model in (39).

### A. Uplink

We assume that orthogonal pilot sequences of length  $n_p^{ul} = 40$  are used in the UL for MMSE channel estimation. Since  $K = 40$ , pilot contamination is avoided. In the centralized case, we use the MMSE combiner [13]

$$\mathbf{u}_i = \rho^{ul} \left( \sum_{i'=1}^K \rho^{ul} (\hat{\mathbf{h}}_i \hat{\mathbf{h}}_i^H + \mathbf{C}_i) + \sigma_{ul}^2 \mathbf{I}_{LM} \right)^{-1} \hat{\mathbf{h}}_i \quad (40)$$

while the local MMSE combiner

$$\mathbf{u}_{il} = \rho^{ul} \left( \sum_{i'=1}^K \rho^{ul} (\hat{\mathbf{h}}_{il} \hat{\mathbf{h}}_{il}^H + \mathbf{C}_{il}) + \sigma_{ul}^2 \mathbf{I}_M \right)^{-1} \hat{\mathbf{h}}_{il} \quad (41)$$

is used with decentralized operation. In (41),  $\mathbf{C}_{il} = \mathbf{R}_{il} - \Phi_{il}$  is the covariance matrix of the estimation error  $\hat{\mathbf{h}}_{il} = \mathbf{h}_{il} - \hat{\mathbf{h}}_{il}$ . MMSE channel estimation is used with both architectures.

1) *Network availability vs. number of antennas*: In Fig. 3, we plot the network availability for  $\rho^{ul} = -10$  dBm, as a function of the total number of antennas  $LM \in \{50, \dots, 400\}$ . We see from Fig. 3 that the centralized cell-free architectures allows one to achieve a network availability  $\eta \geq 0.95$  when  $LM \geq 100$ . Using single-antenna APs ( $M = 1$ ) is optimal in the centralized case: the network availability obtainable for larger values of  $M$  is strictly smaller.<sup>2</sup> This implies that, when providing URLLC services, it is advantageous to distribute as much as possible the available antennas over the coverage area to reduce the average distance between APs and UEs. A cellular architecture with  $L = 4$  BSs requires at least  $M = 64$

<sup>2</sup>The network availability obtainable in the centralized cell-free setting when  $M \in \{2, \dots, 15\}$  is indicated in Fig. 3 by the black dots, which are color-coded from darker ( $M = 2$ ) to lighter ( $M = 15$ ). The same convention is used also in Fig. 6.

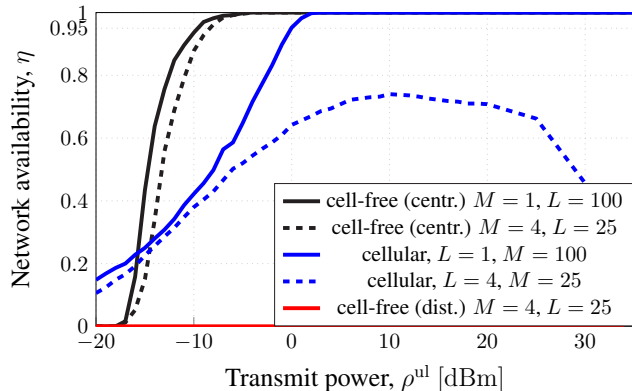
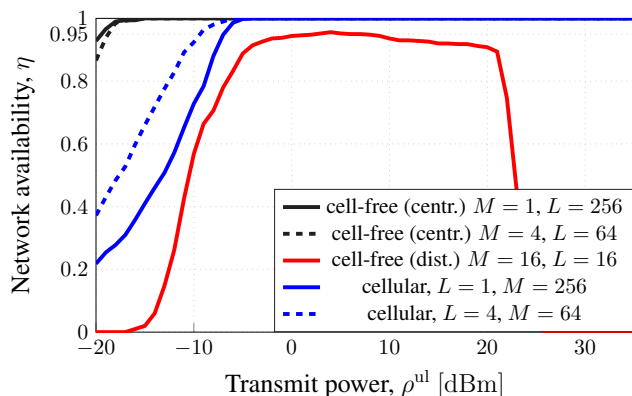
(a)  $LM = 100$ (b)  $LM = 256$ 

Fig. 4: UL network availability as a function of the transmit power for  $LM = 100$  and  $256$ .

antennas per BS (i.e.,  $LM = 256$ ) to achieve  $\eta \geq 0.95$ . This value of network availability cannot be achieved when  $L = 1$ , even when  $M = 400$ , confirming again the importance of reducing the average distance between BSs and UEs. For the values of  $LM$  considered in the figure, the distributed cell-free architecture, whose performance is optimized over  $M \in \{8, \dots, 25\}$ , does not achieve  $\eta \geq 0.95$ . Note that, in this architecture,  $M = 1$  is not optimal. On the contrary, the number of antennas  $M$  per APs (indicated in the figure by the red labels) needs to be increased as  $LM$  is increased to maximize  $\eta$ . This comes as no surprise since (35) provides an accurate channel estimate only when channel hardening occurs, which requires the APs to have sufficiently many antennas.

2) *Network availability vs. transmit power:* In Fig. 4, we plot  $\eta$  as a function of the UL transmit power  $\rho^{\text{ul}}$  for  $LM \in \{100, 256\}$ . For the case  $LM = 100$ , we consider two centralized cell-free architectures, one with  $L = 100$  single-antenna APs and one with  $L = 25$  APs with 4 antennas, as well as two cellular architectures, one with a single BS ( $L = 1$ ) and one with  $L = 4$  BSs. The results of Fig. 4 show that the distributed cell-free architecture does not support positive  $\eta$ . Indeed, the APs have too few antennas to make channel-hardening-based spatial processing work. Furthermore, the centralized cell-free architecture with single-

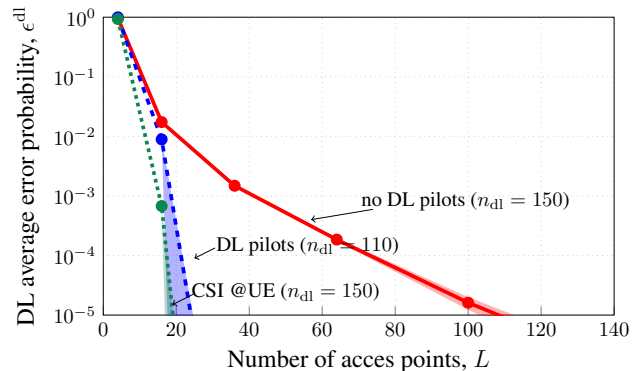


Fig. 5: DL average error probability  $\epsilon^{\text{dl}}$  for the centralized single-user single-antenna cell-free network as a function of the number of single-antenna access points  $L$ . MR precoding is used for transmission.

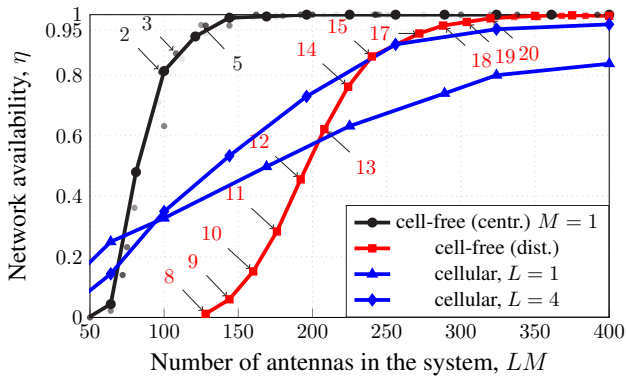
antenna APs achieves  $\eta \geq 0.95$  for  $\rho^{\text{ul}} \geq -17$  dBm. The cellular architecture with  $L = 1$  requires  $\rho \geq 0$  dBm, whereas the cellular architecture with  $L = 4$  is not able to achieve  $\eta \geq 0.95$ , since intercell interference causes a degradation of  $\eta$  when  $\rho^{\text{ul}}$  is increased beyond 10 dBm.

For the case  $LM = 256$ , the performance of both centralized cell-free and cellular improve, as expected. Unlike Fig. 4a, the cellular network with  $L = 4$  outperforms the one with  $L = 1$ . This means that  $M = 64$  antennas are sufficient at each of the 4 BS to provide accurate enough interference management, for the system to benefit from the lower average UE-BS distance. We also illustrate the performance of a distributed cell-free network with  $L = 16$  APs: this architecture does not achieve  $\eta \geq 0.95$ .

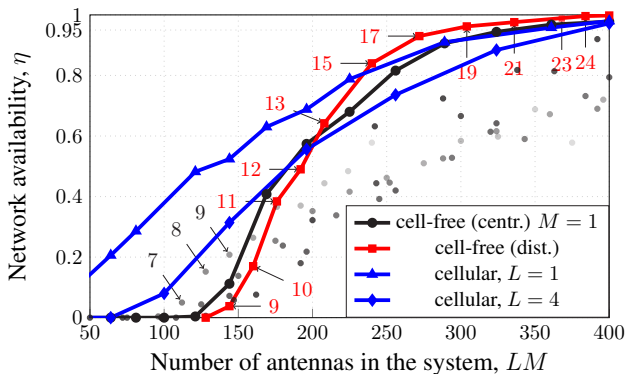
## B. Downlink

We analyze next the DL network availability, with and without DL pilots. When pilot sequences are transmitted, we assume that they are orthogonal and that  $n_p^{\text{dl}} = 40$ , so that  $n^{\text{ul}} = n^{\text{dl}} = 110$ . Furthermore, we assume that the LS channel estimator (29) is used.

1) *The impact of DL pilots:* Before investigating the network availability, we study first the impact of DL pilots for a simple scenario. Specifically, we assume that a single UE is located in the center of the coverage area and analyze the downlink packet error probability achieved by a centralized network with single-antenna APs, with and without DL pilots. MR precoding is used and the transmit power is  $\rho^{\text{dl}} = -10$  dBm. Fig. 5 shows the DL average error probability  $\epsilon^{\text{dl}}$  as a function of the number of APs  $L$ . The case where a genie provides the UE with perfect knowledge of the precoded channel  $g = \mathbf{h}^H \mathbf{w}$  is also reported as benchmark. The figure clearly illustrates that DL pilots are beneficial in a centralized network. Indeed, to achieve an average error probability  $\epsilon^{\text{dl}} = 10^{-5}$ ,  $L = 25$  APs are sufficient. To achieve the same average error probability without DL pilots, one needs  $L = 140$  APs. This means that the penalty incurred by reducing the available channel uses for data transmission from 150 to 110 is much smaller than the benefit from having



(a) With DL pilots



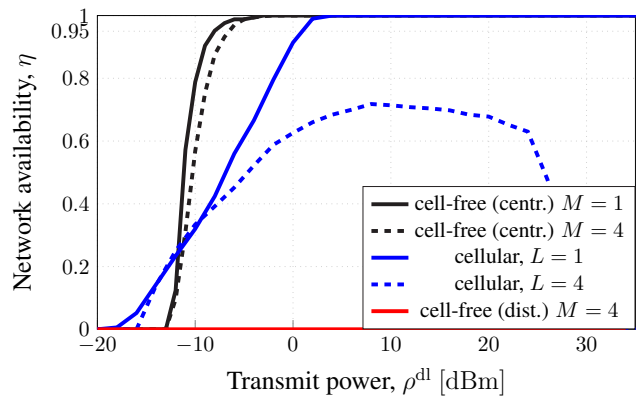
(b) Without DL pilots

Fig. 6: DL network availability for  $\epsilon_{\text{target}}^{\text{dl}} = 10^{-5}$  with MMSE precoding as a function of the total number of antennas in the system,  $LM$ . The labels indicate the number of AP antennas  $M$  necessary to achieve the reported  $\eta$ .

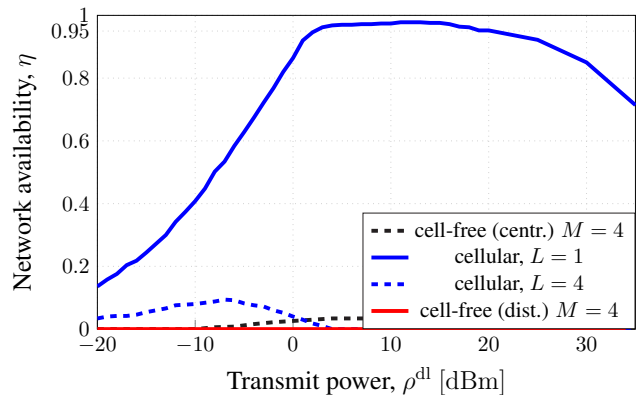
an accurate estimate of the precoded channel  $g = \mathbf{h}^H \mathbf{w}$  at the UE.

2) *Network availability vs. number of antennas*: In Fig. 6a, we show  $\eta$  as a function of the total number  $LM$  of antennas in the system, for the case of DL pilot transmission. For the centralized cell-free and the cellular system, the observations one can draw from the figure are similar to the ones reported for the UL in Section V-A1:  $M = 1$  is almost always optimal in the centralized cell-free case (larger values of  $M$ , which are represented by the other black dots, yield worse performance in general) and  $L = 4$  is superior to  $L = 1$  in the cellular case. The network availability achievable with the distributed cell-free system, optimized over  $M \in \{8, \dots, 25\}$ , is larger than the one achievable in the UL, and this system achieves  $\eta \geq 0.95$  when  $LM \geq 270$ . With the centralized cell-free architecture,  $LM \geq 125$  is sufficient.

When no DL pilots are transmitted (see Fig. 6b), the performance of the cellular network with  $L = 1$  and of the distributed cell-free network actually improves slightly. Indeed, for these two architectures, the use of DL pilots is not beneficial, because the APs are equipped with a sufficiently large number of antennas for channel-hardening-based estimates to be accurate. So it is better to devote the channel uses spent on pilot symbols to data transmission. On the contrary, the performance of the centralized cell-free architecture deteriorates significantly and is inferior to that of



(a) With DL pilots



(b) Without DL pilots

Fig. 7: DL network availability for  $\epsilon_{\text{target}}^{\text{dl}} = 10^{-5}$  with MMSE precoding as a function of the transmit power for  $LM = 100$ .

the distributed cell-free system when  $LM \geq 200$ .

3) *Network availability vs. transmit power*: Fig. 7 shows the DL network availability with and without DL pilots when  $LM = 100$ , as a function of the DL transmit power. For this total number of antennas, the distributed cell-free architecture does not achieve a positive network availability. When DL pilots are transmitted, the performance are similar as the one reported for the UL in Section V-A2: the centralized cell-free with  $M = 1$  in the most performing architecture, and the cellular architecture with  $L = 4$  suffers from multi-cell interference for  $\rho^{\text{dl}}$  larger than around 8 dBm.

When no DL pilots are transmitted, only the cellular architecture with  $L = 1$  is capable of achieving  $\eta \geq 0.95$ . Centralized cell-free with  $M = 4$  (which outperforms the  $M = 1$  centralized architecture) and cellular with  $L = 4$  yield  $\eta \leq 0.1$ .

4) *Do infinite-blocklength metrics provide accurate performance estimates?*: In Fig. 8, we depict the DL network availability computed using as performance metric the outage probability:

$$\mathbb{P} \left[ \log \left( 1 + \frac{\rho g^2}{\sigma^2} \right) < R \right]. \quad (42)$$

The setup is the same as the one considered in Fig. 6a. By comparing Fig. 6a and Fig. 8, we notice that outage probability analyses yield overly optimistic results that can lead to

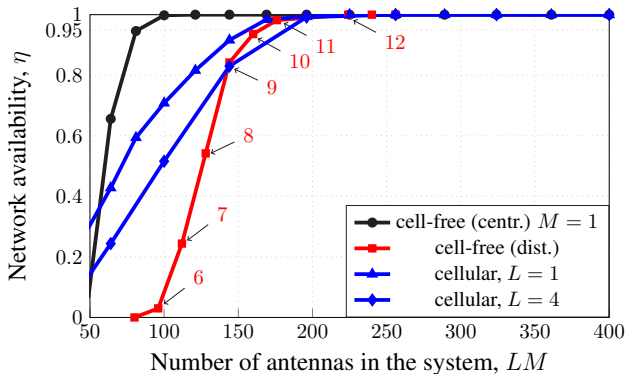


Fig. 8: DL network availability  $\eta$  computed using outage probability with different networks as a function of  $LM$ . The labels indicate the number of AP antennas  $M$  that result in the largest  $\eta$  for the cell-free distributed case.

misleading insights. One can show that similar conclusions hold also for the UL.

## VI. CONCLUSIONS

We analyzed the performance of cell-free Massive MIMO networks supporting the transmission of short packets under the high reliability targets demanded in URLLC. The analysis was carried out using an accurate and easy to evaluate approximation on the per-user UL and DL packet error probability. This approximation relies on the saddlepoint expansion of a finite blocklength bound (see Theorem 1). We showed that the saddlepoint approximation provided in Theorem 2 applies to both cellular and cell-free Massive MIMO networks, thereby generalizing the results by Östman et al. [15]. Hence, while in the asymptotic regime of infinite blocklength, lower bounds on the ergodic capacity are the primary tools to investigate numerically the performance of both cellular and cell-free Massive MIMO systems and derive insights into their design, in this paper we show that, in the short-packet regime, one promising tool to achieve the same goals is the saddlepoint approximation on the RCUs error probability bound (1), computed for the scaled nearest-neighbor decoding rule (2). We used the packet size (blocklength) as a proxy for the latency in the access part of the network. We did not consider the contribution to the latency resulting from processing delay or from transmission of information data over the fronthaul connecting central-processing unit and access point. This is an important issue that is left for future work. It turned out that, in a typical automated-factory scenario, cell-free Massive MIMO with fully centralized processing and single-antenna APs outperforms cell-free Massive MIMO with distributed processing and cellular Massive MIMO. However, for the centralized cell-free Massive MIMO architecture to perform satisfactorily: (i) one must use MMSE linear processing. Indeed, MR processing is not able to guarantee the reliability required in URLLC. (ii) Furthermore, the APs need to transmit precoded pilot sequences in the DL, to allow the UEs to acquire a sufficiently accurate channel estimate. If DL pilots are not transmitted, one has to equip each AP with sufficiently many antennas to induce channel hardening. However, for a fixed total number of antennas per coverage

area, this yields a reduction in the AP density, which affects performance negatively, because of the larger average distance between UEs and APs.

## REFERENCES

- [1] A. Lancho, G. Durisi, and L. Sanguinetti, "Cell-free massive MIMO with short packets," in *Proc. IEEE Int. Workshop Signal Process. Advances Wireless Commun. (SPAWC)*, Lucca, Italy, Sep. 2021.
- [2] 3GPP, "Service requirements for cyber-physical control applications in vertical domains," 3rd Generation Partnership Project (3GPP), Technical Specification (TS) 22.104, 12 2019, version 17.2.0.
- [3] T. L. Marzetta, "Noncooperative cellular wireless with unlimited numbers of base station antennas," *IEEE Trans. Wireless Commun.*, vol. 9, no. 11, pp. 3590–3600, Nov. 2010.
- [4] H. Q. Ngo, E. G. Larsson, and T. L. Marzetta, "Energy and spectral efficiency of very large multiuser MIMO systems," *IEEE Trans. Commun.*, vol. 61, no. 4, pp. 1436–1449, Apr. 2013.
- [5] E. Björnson, J. Hoydis, and L. Sanguinetti, "Massive MIMO has unlimited capacity," *IEEE Trans. Wireless Commun.*, vol. 17, no. 1, pp. 574–590, Jan. 2018.
- [6] E. Björnson, L. Sanguinetti, H. Wymeersch, J. Hoydis, and T. L. Marzetta, "Massive MIMO is a reality—what is next?: Five promising research directions for antenna arrays," *Digital Signal Processing*, vol. 94, pp. 3–20, Nov. 2019.
- [7] E. Björnson, L. Sanguinetti, J. Hoydis, and M. Debbah, "Optimal design of energy-efficient multi-user MIMO systems: Is Massive MIMO the answer?" *IEEE Trans. Wireless Commun.*, vol. 14, no. 6, pp. 3059–3075, Jun. 2015.
- [8] E. Björnson, J. Hoydis, and L. Sanguinetti, "Massive MIMO Networks: Spectral, Energy, and Hardware Efficiency," *Foundations and Trends® in Signal Processing*, vol. 11, no. 3-4, pp. 154–655, Nov. 2017.
- [9] L. Sanguinetti, E. Björnsson, and J. Hoydis, "Towards massive MIMO 2.0: Understanding spatial correlation, interference suppression, and pilot contamination," *IEEE Trans. Commun.*, vol. 68, no. 1, pp. 232–257, Jan. 2020.
- [10] H. Q. Ngo, A. Ashikhmin, H. Yang, E. G. Larsson, and T. L. Marzetta, "Cell-free massive MIMO versus small cells," *IEEE Trans. Wireless Commun.*, vol. 16, no. 3, pp. 1834–1850, Mar. 2017.
- [11] E. Nayebi, A. Ashikhmin, T. L. Marzetta, H. Yang, and B. D. Rao, "Precoding and power optimization in cell-free Massive MIMO systems," *IEEE Trans. Wireless Commun.*, vol. 16, no. 7, pp. 4445–4459, Jul. 2017.
- [12] G. Durisi, T. Koch, and P. Popovski, "Towards massive, ultra-reliable, and low-latency wireless communication with short packets," *Proc. IEEE*, vol. 104, no. 9, pp. 1711–1726, Sep. 2016.
- [13] E. Björnson and L. Sanguinetti, "Making cell-free Massive MIMO competitive with MMSE processing and centralized implementation," *IEEE Trans. Wireless Commun.*, vol. 19, no. 1, pp. 77–90, Jan. 2020.
- [14] Özlem T. Demir, E. Björnson, and L. Sanguinetti, "Foundations of User-Centric Cell-Free Massive MIMO," *Foundations and Trends® in Signal Processing*, vol. 14, no. 3-4, pp. 162–472, 2021.
- [15] J. Östman, A. Lancho, G. Durisi, and L. Sanguinetti, "URLLC with Massive MIMO: Analysis and Design at Finite Blocklength," *IEEE Trans. Wireless Commun.*, vol. 20, no. 10, pp. 6387–6401, Oct. 2021.
- [16] Y. Polyanskiy, H. V. Poor, and S. Verdú, "Channel coding rate in the finite blocklength regime," *IEEE Trans. Inf. Theory*, vol. 56, no. 5, pp. 2307–2359, May 2010.
- [17] A. Martínez and A. Guillén i Fàbregas, "Saddlepoint approximation of random-coding bounds," in *Proc. Inf. Theory Applicat. Workshop (ITA)*, San Diego, CA, USA, Feb. 2011.
- [18] J. Scarlett, A. Martínez, and A. Guillén i Fàbregas, "Mismatched decoding: Error exponents, second-order rates and saddlepoint approximations," *IEEE Trans. Inf. Theory*, vol. 60, no. 5, pp. 2647–2666, May 2014.
- [19] M. Karlsson, E. Björnsson, and E. G. Larsson, "Performance of in-band transmission of system information in massive MIMO systems," *IEEE Trans. Wireless Commun.*, vol. 17, no. 3, pp. 1700–1712, Mar. 2018.
- [20] A. Bana, G. Xu, E. D. Carvalho, and P. Popovski, "Ultra reliable low latency communications in massive multi-antenna systems," in *Proc. Asilomar Conf. Signals, Syst., Comput.*, Pacific Grove, CA, USA, Oct. 2018, pp. 188–192.
- [21] J. Östman, G. Durisi, E. G. Ström, M. C. Coskun, and G. Liva, "Short packets over block-memoryless fading channels: Pilot-assisted or noncoherent transmission?" *IEEE Trans. Commun.*, vol. 67, no. 2, pp. 1521–1536, Feb. 2019.



- [22] W. Yang, G. Durisi, T. Koch, and Y. Polyanskiy, "Quasi-static multiple-antenna fading channels at finite blocklength," *IEEE Trans. Inf. Theory*, vol. 60, no. 7, pp. 4232–4265, Jul. 2014.
- [23] G. Durisi, T. Koch, J. Östman, Y. Polyanskiy, and W. Yang, "Short-packet communications over multiple-antenna Rayleigh-fading channels," *IEEE Trans. Commun.*, vol. 64, no. 2, pp. 618–629, Feb. 2016.
- [24] J. Zeng, T. Lv, R. P. Liu, X. Su, Y. J. Guo, and N. C. Beaulieu, "Enabling ultra-reliable and low-latency communications under shadow fading by massive MU-MIMO," *IEEE Internet of Things J.*, vol. 7, no. 1, pp. 234–246, Jan. 2020.
- [25] H. Ren, C. Pan, Y. Deng, M. ElKashlan, and A. Nallanathan, "Joint pilot and payload power allocation for massive-MIMO-enabled URLLC IoT networks," *IEEE J. Sel. Areas Commun.*, vol. 38, no. 5, pp. 816–830, May 2020.
- [26] J. Zeng, T. Lv, Z. Lin, R. P. Liu, J. Mei, W. Ni, and Y. J. Guo, "Achieving ultrareliable and low-latency communications in iot by fd-scma," *IEEE Internet of Things Journal*, vol. 7, no. 1, pp. 363–378, Jan. 2020.
- [27] A. A. Nasir, H. D. Tuan, H. Q. Ngo, T. Q. Duong, and H. V. Poor, "Cell-free massive MIMO in the short blocklength regime for URLLC," *IEEE Trans. Wireless Commun.*, vol. 20, no. 9, pp. 5861–5871, Sep. 2021.
- [28] G. Interdonato, H. Q. Ngo, P. Frenger, and E. G. Larsson, "Downlink training in cell-free Massive MIMO: A blessing in disguise," *IEEE Trans. Wireless Commun.*, vol. 18, no. 11, pp. 5153–5169, Aug. 2019.
- [29] A. Lancho, J. Östman, G. Durisi, T. Koch, and G. Vazquez-Vilar, "Saddlepoint approximations for short-packet wireless communications," *IEEE Trans. Wireless Commun.*, vol. 19, no. 7, pp. 4831–4846, Jul. 2020.
- [30] P. Yuan, M. C. Coşkun, and G. Kramer, "Polar-coded non-coherent communication," *IEEE Commun. Lett.*, vol. 25, no. 6, pp. 1786–1790, Jun. 2021.
- [31] W. Feller, *An Introduction to Probability Theory and Its Applications*, 2nd ed. New York, NY, USA: Wiley, 1971, vol. II.
- [32] A. Lapidoth and S. Shamai (Shitz), "Fading channels: How perfect need 'perfect side information' be?" *IEEE Trans. Inf. Theory*, vol. 48, no. 5, pp. 1118–1134, May 2002.
- [33] G. Grimmett and D. Stirzaker, *Probability and Random Processes*, 3rd ed. Oxford University Press, 2001.
- [34] A. O. Kislal, A. Lancho, G. Durisi, and E. Ström, "Efficient evaluation of the error probability for pilot-assisted URLLC with Massive MIMO," Nov. 2022. [Online]. Available: <http://arxiv.org/abs/2211.02385>